Spatial/spectral encoding of the spin interactions in ultrafast multidimensional NMR

Yoav Shrot[a] and Lucio Frydman[b]
Department of Chemical Physics, Weizmann Institute of Science, Rehovot 76100, Israel

(Received 3 September 2009; accepted 29 October 2009; published online xx xx xxxx)

Two-dimensional nuclear magnetic resonance (2D NMR) spectroscopy provides the means to extract diverse physical, chemical, and biological information at an atomic level. Conventional sampling schemes, however, may result in relatively long 2D experiments; this has stimulated the search for alternative, rapid acquisition schemes. Among the strategies that have been recently proposed for achieving this counts an "ultrafast" approach, relying on the spatial encoding of the indirect domain evolution to provide arbitrary spectra within a single scan. A common feature of all spatial encoding schemes hitherto described is their uniform encoding of a continuous bandwidth of indirect-domain frequencies, regardless of the chemical sites' spectral distribution within it. These very general conditions, however, are often associated with a number of tradeoffs and compromises in the spectral widths and resolutions that can be achieved for both the direct and indirect domains. This paper proposes a different strategy for single-scan acquisition of 2D spectra, which performs an optimal encoding by employing *a priori* information regarding the positions of NMR resonances along the indirect domain. We denote this as "spatial/spectral encoding"; the underlying principles of this new approach, together with experimental results based on uni- and multidimensional rf pulse schemes, are presented. © *2009 American Institute of Physics*. [doi:10.1063/1.3266422]

I. INTRODUCTION

Two-dimensional nuclear magnetic resonance (2D NMR) spectroscopy serves as a powerful tool to obtain information about structure and dynamics in chemistry and biochemistry.[1,2] This class of experiments is routinely used for identifying the components comprising a sample under investigation as well as for unraveling the scaffolding of unknown chemical structures. Various methodologies have been devised to extract this variety of information;[3,4] the overwhelming majority of these share a basic scheme based on the general proposal by Jeener and Ernst for the collection of 2D NMR data,[5,6]

$$\text{Preparation-Evolution}(t_1)\text{-Mixing-Acquisition}(t_2). \quad (1)$$

According to this paradigm, the spins evolve as a function of two time variables. The ν_1 indirect domain is monitored via the introduction of a delay parameter t_1 that is uniformly incremented in a series of independent experiments. For each value of t_1, the spins' response as a function of t_2 [the free induction decay (FID)] is then monitored along the direct domain t_2. Proper rearrangement of the resulting set of FIDs $\{S(t_1,t_2)\}$, followed by a numerical 2D Fourier transformation (FT), provides the 2D $I(\nu_1,\nu_2)$ spectrum correlating the spin frequencies that were active during the indirect-domain and direct-domain evolutions. The spectra resulting from this procedure are characterized by independent spectral widths $(\mathrm{SW}_1,\mathrm{SW}_2)$ and spectral resolutions $(\Delta\nu_1,\Delta\nu_2)$ along the corresponding frequency axes. These will be given, respectively, by

$$(\mathrm{SW}_1,\mathrm{SW}_2)=\left(\frac{1}{\Delta t_1},\frac{1}{\Delta t_2}\right);$$
$$(\Delta\nu_1,\Delta\nu_2)=\left(\frac{1}{N_1\Delta t_1},\frac{1}{N_2\Delta t_2}\right). \quad (2)$$

Here Δt_1 is the delay used to increment the indirect-domain time parameter, Δt_2 is the acquisition dwell time, N_1 is the number of distinct t_1 increments that were used, and N_2 is the number of points collected in the FIDs. Although Δt_1, Δt_2, and N_2 can usually be set more or less arbitrarily without penalties (other than for the limits set by the relaxation times T_2), N_1—which linearly defines the total time allocated to the experiment's duration—may be a taxing parameter to set. Indeed, it follows from Eq. (2) that when not bound by sensitivity considerations, attempting to achieve high $\Delta\nu_1$ spectral resolutions while faithfully covering large SW_1 bandwidths (BWs) requires N_1 to be large, and therefore demands the acquisition of numerous independent scans.

Over the years various strategies have been suggested to ameliorate this sampling-imposed limitation, and to minimize the total experimental duration without compromising on spectral resolution and/or the BW of interest. Some of these approaches are "passive," relying for instance on letting peaks simply fold over along the indirect domain.[7,8] *A priori* information about the indirect-domain spectrum can then be used to provide the exact positions of the peaks along this axis. Another active approach that also exploits prior information about the desired ν_1-spectral lines involves exciting these chemical sites of interest in a selective

[a]Electronic mail: yoav.shrot@weizmann.ac.il.
[b]Tel.: +972-8-9344903. FAX: + 972-8-9344123. Electronic mail: lucio.frydman@weizmann.ac.il.

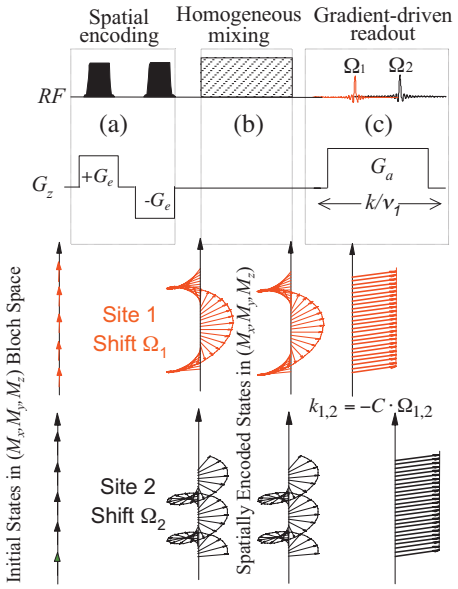

FIG. 1. Principles of ultrafast 2D NMR. Spatial encoding creates a linear relation between position z and evolution time t_1; different chemical sites therefore generate different helical patterns depending on their chemical shift. This spatial information is preserved throughout the coherence mixing period. Integrating the contribution of all the spins in the sample at the beginning of the acquisition stage provides a recorded signal of negligible amplitude. But a gradient possessing the same geometry as used in the encoding stage can unwind this spatial profile and generate echoes whose timing varies linearly with the indirect-domain frequency.

fashion.[9,10] Given N such sites, one then needs only N one-dimensional (1D) FIDs to unambiguously resolve the direct-domain spectrum for each of the indirect-domain peaks of interest, and hence for reconstituting the 2D NMR information. Other alternatives involve departing from FT processing, and employ nonuniform mapping of the indirect domain to bypass the strict demands of Eq. (2).[11–15] Although all these approaches require less repetitions than their conventional counterparts, they may still demand a considerable number of scans when attempting to characterize multiple spreadout sites with high spectral resolution.

An alternative general approach to reduce the number of experiments of a 2D NMR all the way down to a single scan is provided by so-called "ultrafast" NMR methods.[16,17] In these schemes (Fig. 1) all t_1 values are spatially encoded into the sample in parallel, thus compressing the whole series involved in a 2D acquisition into a single scan. The corresponding phases of the transverse spin magnetizations at the beginning of the t_2 acquisition will be given in these experiments by spatially dependent factors of the form[17,18]

$$\phi(z) = \Omega_1 t_1(z) = \Omega_1 t_1^{\max} \frac{z - z_0}{L} = C\Omega_1 (z - z_0), \tag{3}$$

where L is the encoded sample's length, Ω_1 is the indirect-domain shift one is trying to measure, and $t_1^{\max}$ is the effective overall evolution time. During the FID recording time, the encoded information is acquired while in the presence of $\pm G_a$ oscillating gradients that map the spins' response as a function of $[k(t_2), t_2]$, where $k(t) \equiv \gamma_a \int_o^t G_a(t')dt'$. Denoting the 2D spectral correlation being sought as $I(\Omega_1, \Omega_2)$ and neglecting for simplicity relaxation effects, the resulting signal is given by

$$S(k,t_2) \propto \int_L dz \left[\int_{\nu_1} \int_{\nu_2} d\Omega_1 d\Omega_2 I(\Omega_1,\Omega_2) e^{iC\Omega_1 z} e^{i\Omega_2 t_2} \right] e^{ikz}. \tag{4}$$

The integration over the spatial dimension will provide a negligible signal, except for k-values that match the positions of the indirect domain spectral lines, i.e., $k = -C\Omega_1$. Thus, in practice, the k-axis linearly maps the entire ν_1 indirect domain. The $\pm G_a$ oscillating gradient waveform repeatedly monitors these echo trains and their corresponding train of spectra $I(\Omega_1) - 2N_2$ times as a function of t_2. Proper rearrangement of the data and application of a 1D FT along t_2 thus provide the full 2D NMR spectrum being sought within a single scan.

When setting up the various parameters of such ultrafast 2D NMR acquisitions,[19] one needs to consider variables that both match and differ from those arising in conventional 2D experiments. As in Eq. (2), $2T_a = \Delta t_2$ and N_2 will define the FT-derived ν_2-domain axis. SW_1 and $\Delta\nu_1$, by contrast, will involve the G_a's amplitude and the timings involved throughout the various stages of the experiment. Given the linear relation in Eq. (3), and taking the acquisition gradient half-cycle period and constant amplitude to be T_a and G_a, respectively, the spectral width to be scanned along the indirect domain will be $\mathrm{SW}_1 = k^{\max}/C = \gamma_a G_a T_a / C$. As for the indirect domain resolution $\Delta\nu_1$, the echo shape as a function of k for a uniform spin distribution of length L is proportional to $\mathrm{sinc}(kL/2)$, which provides a typical echo width of the order of L^{-1}.[20] When translating this indirect-domain $\Delta k \approx L^{-1}$ resolution from k-terms into frequencies, one obtains that $\Delta\nu_1 = \Delta k / C \approx 1/t_1^{\max}$. It follows from all this that for a given set of SW_1, SW_2, and $\Delta\nu_1$ demands, the acquisition gradient G_a should be set to fulfill

$$\gamma_a G_a L = \frac{CL \cdot \mathrm{SW}_1}{T_a} = 2\frac{\mathrm{SW}_1 \cdot \mathrm{SW}_2}{\Delta\nu_1}. \tag{5}$$

$\gamma_a G_a L$ also defines the receiver's BW that will have to be covered in this kind of experiments. Indeed, by contrast to conventional acquisitions where BW is simply set by SW_2, ultrafast experiments will demand an increased BW value for the simultaneous sampling of the two spectral domains. Such demand leads to a degradation of the signal to noise ratio (SNR) on a per-scan basis according to a BW-dependent noise factor of

$$\mathrm{SNR} \propto \frac{1}{\sqrt{\mathrm{BW}}} \approx \frac{1}{\sqrt{\gamma_a G_a L}} = \sqrt{\frac{\Delta\nu_1}{2\mathrm{SW}_1\mathrm{SW}_2}}. \tag{6}$$

Equations (5) and (6) summarize the main bottlenecks of the ultrafast spatial encoding method. Indeed Eq. (5) indicates that acquiring data spanning large spectral regions while demanding a high ν_1 spectral resolution will require the availability of strong acquisition gradients. This can be a limiting hurdle, especially if the NMR probehead being used is not equipped with customized gradients, or when demanding the high duty cycles that may be necessary to follow

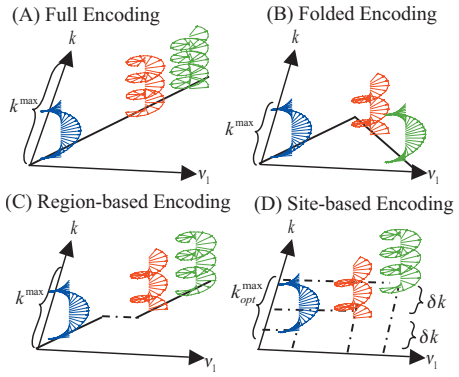

FIG. 2. Strategies for spatial encoding the indirect spectral domain illustrated for three chemical sites assumed unequally spaced along the frequency axis (with one far apart from the other two). (a) Conventional mapping creating a linear relation between ν_1 and k. This general linear mapping necessitates a strong acquisition readout gradient covering a large k-range. (b) A reduction in the k-range to be scanned is possible by "folding" frequencies into a confined k-region and using multiple scans (two in this figure) to "unfold" the spectrum. (c) Using *a priori* information about the spectral peaks, a selective encoding can be used to exclude empty ν_1-ranges and encode only the regions of interest. (d) An optimal encoding can be obtained if a discrete set of frequencies is excited and encoded with a minimal winding separation δk, leading to a minimal k-range to be scanned.

rapid real-time kinetic acquisitions. Moreover, even if the gradient hardware demands can be fulfilled, Eq. (6) highlights the sensitivity penalties that will still arise in such cases due to the noise's variance increase with the gradient's amplitude.

The limitations just highlighted will often materialize for indirectly detected characterizations of natural abundance organic samples. In such cases one commonly intends to characterize the large SW_1 spectral regions associated with ^{13}C or ^{15}N nuclei, with a high $\Delta\nu_1$ resolution. SNR is also a major issue in this kind of experiments. Fortunately, an opportunity to alleviate these limitations also arises when dealing with such cases due to the "sparse" nature of the data; i.e., due to the presence of large bands of the indirect domains known *a priori* to be empty. Uniformly scanning such empty regions with high spectral resolution in the usual spatial encoding mode leading to Eqs. (5) and (6) [Fig. 2(a)] is onerous both in terms of gradients and of sensitivity. A somewhat analogous situation arises in conventional 2D spectroscopy, where a high number of N_1 experiments will be needed [Eq. (1)] even when dealing with empty ν_1 regions. In conventional 2D NMR this demand can be ameliorated by folding/unfolding procedures;[7,8] similarly, folding and unfolding of the indirect-domain spectral regions can also be used in spatially encoded spectroscopy to alleviate the above-mentioned demands. Examples of such methods have been demonstrated,[21,22] whereby different mapping schemes were used to "fold" m different subspectra into a reduced region of k-space [Fig. 2(b)]. At the cost of conducting multiple scans, these different spectral regions can be subsequently separated and the indirect domain faithfully reconstructed. Although these procedures require reduced gradient amplitudes they demand multiple scans, and may thus be unsuitable for situations where single scans are of essence. In such cases an alternative mapping scheme like that introduced in Fig. 2(c) would be preferable. This scheme partitions the indirect domain into relevant and irrelevant spectral regions. The former are then spatially encoded with the desired linear dephasing, while the latter remains in practice excluded from the spatial encoding. Under such conditions the k-range that one needs to scan for unraveling the spectral information becomes considerably smaller than that required to cover the full SW_1. For a given SW_2 this then leads to reduced G_a demands, bypassing all the problems listed earlier. In fact an optimal reduction in the k-range to be scanned would result if the spectral regions of interest could be encoded on a site-by-site basis. In such case the ν_1-k mapping could be modified into a discrete, ideal $\{\Omega_p \leftrightarrow k_p\}_{p=1\cdots N}$ scheme like the one illustrated in Fig. 2(d). Given N sites to be resolved and denoting the minimally resolvable separation along the k-axis as δk (a wave-number on the order of L^{-1}), the k-range to be scanned would then be given by an optimal value $k_{\text{opt}}^{\text{max}} = N\delta k$. Assuming N is considerably smaller than $N_1 = SW_1/\Delta\nu_1$, the necessary acquisition gradient could then be set significantly smaller than what is needed by conventional ultrafast 2D NMR: a reduction by $\sim N/N_1$. Such improvement is akin to that involved in Hadamard-based spectroscopy,[3,10] except that instead of affecting the minimal number of experiments, it would reduce the gradient and SNR penalties associated with the monitoring of a broad SW_1 with high resolution. Several alternative strategies to implement this new spectral/spatial mapping of the indirect domain are discussed in Sec. II, some of them considerably simpler than any encoding approach hitherto suggested. Section III follows by demonstrating the applicability of these approaches and their benefits compared with the conventional, uniform spatial encoding used in 2D ultrafast acquisitions. Section IV concludes by discussing the performance limitations, potential advantages, and possible applications of the new approaches.

II. SPECTRALLY SELECTIVE SPATIAL ENCODING SCHEMES

It follows from Sec. I that spatial encoding relies on endowing each Ω_p site with a spatial winding, such that its corresponding echo will be generated during the acquisition at a different position along the k-axis. Such echoes are considered resolvable if they do not overlap with one another. Denoting this minimally resolvable k-separation by δk, an optimal allocation of the winding patterns calls for equally distributing the $\{\Omega_p\}_{p=1\cdots N}$ peaks to be resolved at distances δk apart. Given these conditions, the range to be scanned during each direct-domain dwell period becomes $k_{\text{opt}}^{\text{max}} = N\delta k$, and our encoding goal can be summarized by the one-to-one allocation

$$\Omega_p \mapsto k_p = (p - N/2)\,\delta k, \quad p = 1,2,\ldots,N. \tag{7}$$

Having decided on a minimal δk, the objective given by Eq. (7) can then be realized by two different approaches: one uses a strategy based on a discrete, sequential addressing of the frequencies to be encoded; the other addresses all the targeted frequencies simultaneously. We discuss these two cases separately.

(A) Serial Spatial/Spectral Encoding (SSE) (B) Parallel Spatial/Spectral Encoding (PSE)

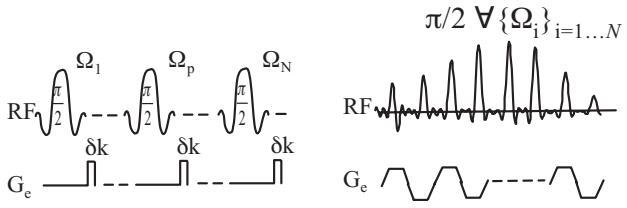

SCHEME 1.

A. Implementing a serial spectral/spatial encoding of the sites

Scheme 1(a) illustrates a simple route to implementing the encoding required by Eq. (7). This serial selective encoding (SSE) scheme employs a train of selective pulses that sequentially excite each of the $\{\Omega_p\}_{p=1\cdots N}$ sites of interest, and interleave these rf manipulations with a train of identical gradient pulses characterized by the minimal wave-number separation δk. Every chemical site, being excited at a different stage of the encoding period, experiences a different number of gradient pulses; sites become thereby linearly encoded by winding patterns of different pitches, as determined by their order of excitation. Assuming a pth selective rf pulse that excites a spectrum characterized by a profile of $Q(\nu_1 - \Omega_p)$, the final magnetization arising from Scheme 1(a) will be given by

$$M_{XY}(z,\nu_1) \propto \sum_{p=1}^{N} I(\nu_1)\exp[i(N-p+1)\cdot \delta k z]Q(\nu_1-\Omega_p), \tag{8}$$

where $I(\nu_1)$ is proportional to the spectral distribution at a shift ν_1. Aiming to address each chemical site selectively requires that the length of each of the constituent rf pulses defining $Q(\nu)$ be made inversely proportional to the targeted spectral resolution. Although arguably the simplest of all spatial encoding schemes proposed so far, this SSE approach suffers from a number of drawbacks. In particular, if some of the targeted frequencies are close to one another, if dealing with numerous N sites, or if suffering from short T_2 transverse relaxation times, this sequential excitation approach may lead to considerably long pulse durations and to ensuing relaxation losses of the various sites over the encoding stage. The origin of this problem lies in the serial way by which the individual sites are encoded; we turn next to an approach that performs the same encoding in a parallel, simultaneous way.

B. Parallel spectral/spatial encoding

The second approach to be discussed uses a strategy whereby all the chemical sites are endowed with their specific dephasing factors simultaneously, making Eq. (7) true for all Ω_p's at the same time. Such parallel selective encoding (PSE) [Scheme 1(b)] realizes this kind of manipulations on the basis of so-called 2D spatial-spectral rf pulses.[23,24] These rf pulses find ample use in magnetic resonance imaging, where they are employed to selectively excite/invert spins of interest, both according to their chemical shift (e.g., water or fat) as well as according to their spatial position. In contrast to this pattern, the 2D spatial/spectral pulses designed for the purposes of the present study will have as objective to endow the sample with a response in the ν_1-z plane, according to a targeted winding pattern

$$M_{XY}^{\text{desired}}(z,\nu_1) = \sum_{p=1}^{N} \exp(ik_p z)Q(\nu_1-\Omega_p), \tag{9}$$

where Q is the local windowing function introduced in Eq. (8). According to the linear, small-tilt-angle approximation,[25,26] the shaped rf pulse capable of delivering this spectral/spatial pattern will also have to fulfill the condition

$$M_{xy}(z,\nu_1) \propto \int_0^{T_{\text{pulse}}} B_1(t)\exp[-i(k(t)\cdot z + t\nu_1)]dt. \tag{10}$$

On the basis of this demand one can calculate the irradiation field function $B_1(t)$ delivering the 2D profile in Eq. (9) for arbitrary trajectories in k-space. Indeed, the availability in Eq. (10) of two degrees of freedom (k and t) discriminating the spatial and spectral components defining the spin evolution provides the flexibility needed for imposing the pattern in Eq. (9) from a single continuous pulse. The Appendix gives further details on these spatial/spectral manipulations, including information on how this kind of rf pulses was calculated and implemented in the present study. Among the general features associated with such 2D rf pulses is the fact that the typical spectral resolution of Q will, like the spectral resolution of any selective pulse, be inversely proportional to the pulse's duration T_{pulse}. Unlike in the SSE case, however, where the overall preparation time was given by the *sum* of the individual rf and gradient pulse durations needed to excite the various chemical sites, in the PSE scheme all sites are addressed simultaneously. The total excitation time is thus equal to the preparation time necessary to excite an individual site. The major advantage of this is that the signal losses arising from T_2 relaxation effects or from homonuclear J-coupling modulations during the encoding period become considerably ameliorated. On the negative side, the design and applications of these rf waveforms and gradient waveforms are naturally more complex than the very simple encoding steps involved in the SSE. Also, from an experimental performance perspective, the fact that a continuously oscillating gradient is needed in PSE will often require stronger gradients to obtain the same desired spatial phase encoding pattern, as that given by the simple N pulsed-gradient SSE approach. Still, as demonstrated in Sec. III, this does not constitute a limitation for practical PSE applications. For completion, benefits and drawbacks of the various new encoding methods considered in this study vis-à-vis those of the conventional spatial encoding method are summarized in Table I.

III. RESULTS

A. Experimental methods

In order to test the various considerations just presented, a series of experimental comparisons was made between spa-

TABLE I. Pros and cons of spatial and spatial/spectral encoding methods.

	Conventional spatial encoding	Sequential spectral-spatial encoding	Parallel spectral-spatial encoding
Pros	General	Simple to use	Short encoding times
		Weak encoding gradients	Uniform relaxation weighting
		Optimally exploited k-range	Optimally exploited k-range
		→ Best SNR and weakest G_a	→ Best SNR and weakest G_a
Cons	$\frac{SW_1SW_2}{\Delta\nu_1} \propto \gamma_a G_a L$	Needs *a priori* information	Needs *a priori* information
	→ Strong acquisition gradients and low SNR for sparse ν_1 domains	Possibly long encoding time	Strong encoding gradients
		Nonuniform relaxation	Nontrivial pulse design

tial and spatial/spectral encoding methods. These measurements were carried on a 11.7 T magnet equipped with a HCN probe and a Varian iNova® NMR console. The pulses and gradient waveforms required by the various experiments were generated via custom-written MATLAB codes (available upon request), so were all the data rearrangement and processing manipulations. The experiments implemented for these studies were divided into two groups, seeking to explore the two main potential advantages of SSE and PSE spatial/spectral encoding. A first set of tests used heteronuclear single quantum correlation (HSQC) 2D experiments to explore the potential SNR improvements which could arise upon using the new scheme in the analysis of simple organic molecules. A second set of tests employed homonuclear ^{1}H–^{1}H J-mediated total correlation spectroscopy (TOCSY) experiments to explore the results arising from spatial/spectral encoding in cases where the ν_1 resolution may be dictated by the maximal acquisition gradient amplitudes available.

B. SNR and resolution improvements: Heteronuclear 2D NMR correlation examples

One of the improvements expected from the new spatial/spectral encoding protocols relates to their need for weaker G_a gradients. This should increase the SNR [Eq. (6)], allowing for G_a's that operate longer acquisition times, and bringing in turn improvements in the ν_2 resolution. To test all this a series of heteronuclear 2D ultrafast ^{13}C–^{1}H HSQC NMR experiments was performed on a sample containing a mixture of 1-butanol and *n*-butyl chloride at natural abundance dissolved in $CDCl_3$. The 1D ^{13}C spectrum of this mixture contains eight sites spanning over 50 ppm showing a variety of spacings, making it a good representative of the challenges mentioned earlier. A purely absorptive ultrafast 2D HSQC of this sample, designed to include all the chemical sites without aliasing, is shown in Fig. 3. The relatively broad spectral ranges of both ^{1}H and ^{13}C in this 2D spectrum demanded the use of relatively strong acquisition gradients: $|G_a| \approx 45$ G/cm. Even under these conditions we had to compromise on a number of factors, including the indirect-domain evolution time (t_1^{max} of only 8 ms) and the total FID acquisition time (t_2^{max}=46 ms). These choices resulted in reduced spectral resolutions along both the indirect and direct domains, as well as in SNR losses due to the broad receiver BW and short acquisition times involved [Fig. 3(b)].

Figure 4 illustrates an application of the SSE protocol to this same system. The ^{13}C domain included eight chemical sites (Fig. 3); as the two sites located near 34.7 ppm have a very small gap in between them (~0.05 ppm, 6 Hz), no efforts were made to distinguish among these. All remaining ^{13}C sites could be well separated if addressed independently by a train of reasonably short (~15 ms) rf pulses. Following each of these resulting seven selective pulses, gradient pulses characterized by $\delta k = 1.2L^{-1}$ wave-numbers were applied to evenly distribute their corresponding spatial encodings. This enabled us to set the acquisition k^{max} to the lowest value compatible with a seven-peak spectrum, thus decreasing the value needed for G_a from 45 to 9.4 G/cm. This decrease enabled in turn a much longer acquisition time (~350 ms)

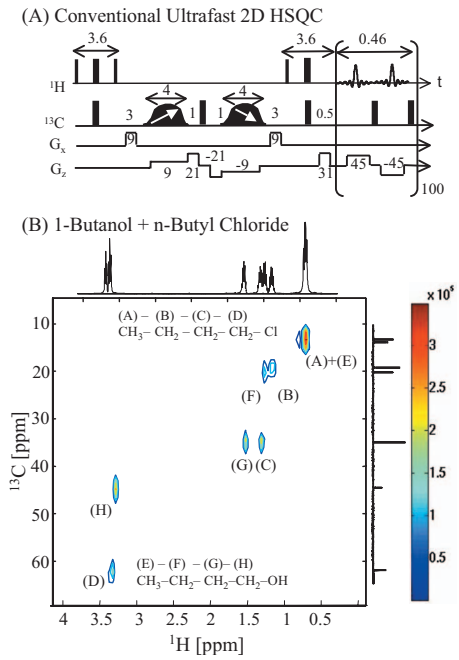

FIG. 3. (a) Conventional spatially encoded 2D HSQC experiment on a mixture of 1-chlorobutane and 1-butanol based on a sequence employing two oppositely sweeping $\pi/2$ chirped pulses, separated by a hard π pulse that provides purely absorptive line shapes (Ref. 34). (b) Ultrafast 2D ^{13}C–^{1}H correlation spectrum (real components). The acquisition dwell time used here and throughout all the experiments in this paper was 5 μs; spectral resolution along the ν_1 axis was 200 Hz. Like throughout all the remaining pulse sequence diagrams in this paper, gradient amplitudes and timings provided in this figure are in units of G/cm and millisecond, respectively; nonselective $\pi/2$ and π pulses are symbolized by thin and thick lines, respectively; arrowed pulses indicate frequency-chirped rf blocks; brackets show events looped over the indicated number of times.

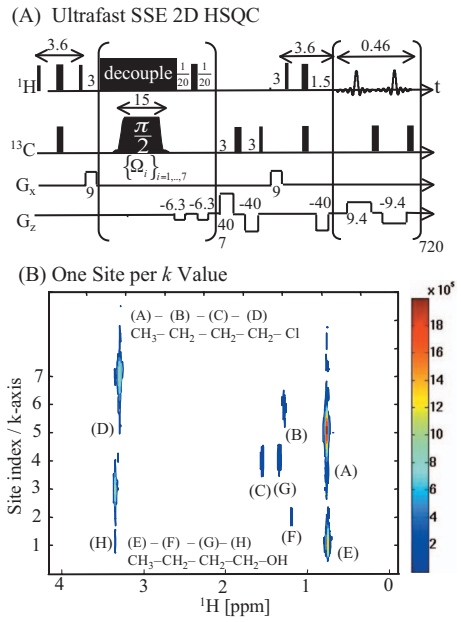

FIG. 4. (a) Serially selective excitation scheme employing a train of selective rf pulses interleaved with gradient pulses to perform a spatial/spectral encoding. In order to get a narrow-banded response, pulses of 15 ms were designed by the Shinnar–Le Roux algorithm (Ref. 35), providing an excitation BW of ~75 Hz. Following each pulse a gradient pulse (split for ^{1}H-decoupling purposes) endowed the excited sites with uniform increments in their wave-numbers. Acquisition of a 2D spatially encoded HSQC spectrum (b) could thus be achieved using considerably weaker G_a gradients (display in absolute-value mode).

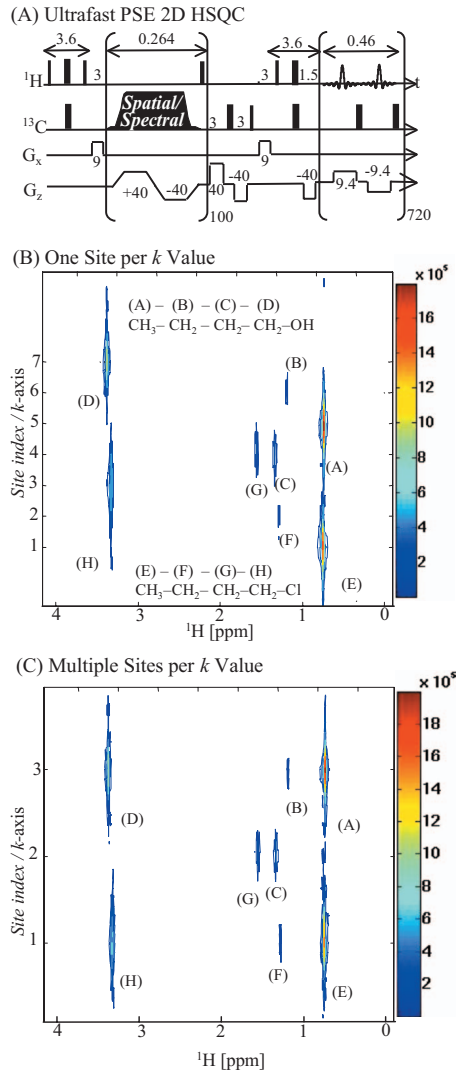

FIG. 5. (a) Parallel selective excitation protocol designed with a performance akin to the sequence in Fig. 4 except for its addressing of all the spins simultaneously. The flexibility of the spatial-spectral encoding can be used to either (b) endow every site with a different k wave-number or (c) arrange the sites in fewer, further separated groups, providing a better resolution along the indirect domain. Images are displayed in absolute-value mode and indicate the positions ascribed to each chemical site along the k-axis.

bringing about a better $\Delta\nu_2$ resolution and a substantial increase in the signals' intensities. Notice that despite the long duration taken by the discrete selective pulses in this SSE test (~100 ms), the long T_2's characterizing the ^{1}H-decoupled ^{13}C evolution implied only minor losses: peak intensities were thus nearly independent from the order of excitation of the various sites. This fact, coupled to the small encoding wave-number δk used (6.3 G/cm, 0.1 ms), implied that neither diffusion nor relaxation should have had much of an influence during the encoding. In cases such as this, the difference in signal intensity arising upon using the SSE or the PSE approaches should be minor. To test this hypothesis, the parallel approach was implemented using a 2D spatial spectral rf pulse designed to endow the various sites in the sample with an encoding pattern identical to that employed for the SSE. The total encoding duration could be thus made considerably shorter, reducing it from ~100 to ~25 ms, even if at the expense of much stronger oscillatory gradients [Fig. 5(a)]. The resulting 2D ultrafast spectrum [Fig. 5(b)] showed, in terms of both SNR and G_a requirements, a similar performance as the results shown in Fig. 4(b) upon using the SSE method.

Besides a higher efficiency in their use of gradients, the new spectral/spatial methods offer a potential encoding flexibility that is just absent in the traditional spatial encoding methods. These variations include, for example, spectral/spatial encoding profiles that do not necessarily endow each chemical site with a different encoding wave-number: one could then provide certain chemical sites that are known to be resolved in ν_2 with identical k's wave-numbers. The reduced number of encoding δk wave-numbers could then allow either the use of even weaker acquisition gradients, or a better separation in k/ν_2 by an increase in δk without compromising the effective resolving power of the 2D experiment. Figure 5(c) illustrates an example of this: it shows the use of an alternative PSE scheme, endowing the eight sites in the mixture with only three k-values in their spatial encodings. Using the same excitation and acquisition gradients one can then spread the indirect domain further apart to $\delta k = 3.6L^{-1}$ in this example and achieve a correspondingly better resolution without increasing G_a. Another variant of the PSE approach is displayed in Fig. 6(a), which introduces a sequence aiming to obtain the same spatial encoding as in Fig. 5(c), but operating in a purely absorptive acquisition mode. This can be achieved while retaining the experiment's single-scan character by employing spatial/spectral pulses as part of both the HSQC's indirect domain excitation as well as of its storage stages—with a hard 180° pulse inserted in between.

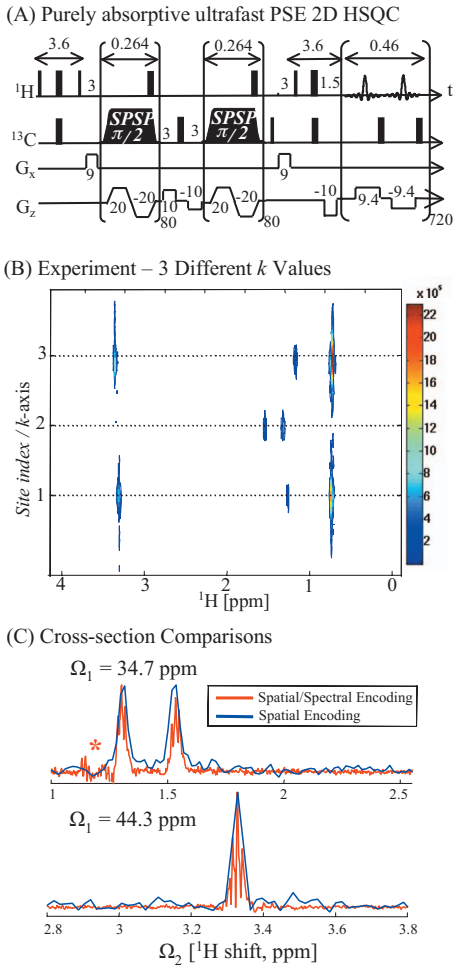

FIG. 6. (a) Pulse sequence encoding purely absorptive spectroscopy based on a variation in the PSE scheme, whereby spatial/spectral pulses are used for both excitation and storage of magnetization. (b) Purely absorptive 2D HSQC spectrum collected using only three k-values along the ^{13}C dimension [akin to Fig. 5(c)]. (c) Normalized ν_2-cross sections extracted for the indicated indirect-domain ppm frequencies, comparing the results arising from the purely absorptive 2D HSQC NMR spectra in (b) and Fig. 3(b). An improvement of both SNR and direct domain resolution is evident. The asterisk (*) indicates a minor cross-talk caused by an overlap with the adjacent CH_2 echoes.

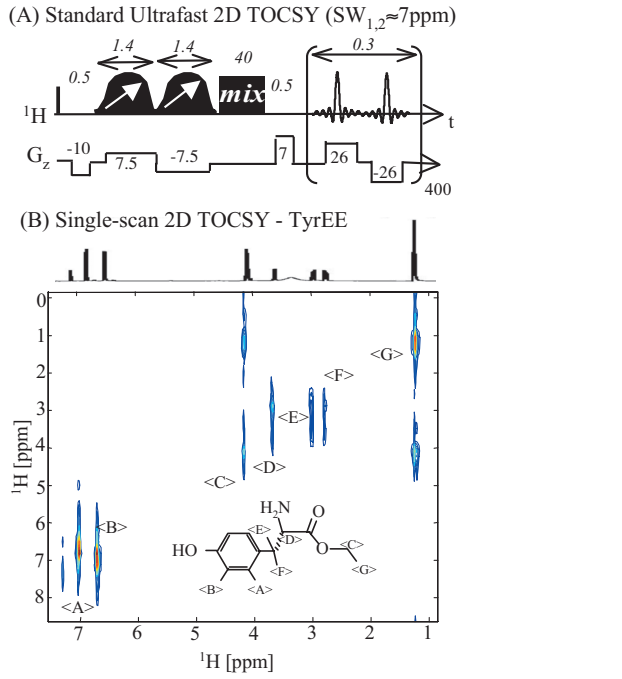

FIG. 7. (a) Conventional spatially encoded ^1H TOCSY experiment on a sample of tyrosine ethyl ester dissolved in $CDCl_3$. (b) Spectrum displayed in absolute-value mode. In order to enable large direct-domain BW and resolution, a moderate acquisition gradient was necessary and a tradeoff with respect to the indirect-domain resolution had to be made.

The latter's role is to cancel any linear chemical shift phase evolution as well as pulse imperfections while the spatial dephasing is accumulated. Due to the "doubled" character of the ensuing encoding, a gradient that is only half the amplitude of the nonsymmetric counterpart (20 versus 40 G/cm) and shorter pulses can provide the same degree of desired encoding with a better line shape and sensitivity [Fig. 6(b) versus Fig. 5(c)].

All the spatial/spectral implementations described in Figs. 5 and 6 allowed us to reduce the acquisition gradient vis-à-vis the values required by the original spatial encoding experiment by a factor of ~5. This was achieved at no cost in the ν_1 resolution and enabled in turn two concurrent improvements: (1) the use of longer acquisition times, made possible thanks to the weaker G_a's involved, and (2) lower noise levels, thanks to the accommodation of reduced receiver BWs of $\sim\gamma_a G_a L$. The combination of these two factors should increase the direct-domain spectral resolution and provide a considerable sensitivity improvement. Figure 6(c) evidences these two features by displaying normalized 1D cross sections extracted from both the purely absorptive spectral/spatial PSE encoding scheme and from a traditional spatially encoded 2D purely absorptive HSQC spectrum. The enhancement in resolution (notice the clear homonuclear J-coupling patterns) and decrease in noise are evident. Furthermore, even if SNR is not the limiting constraint in the ultrafast 2D acquisition, one can use the tools afforded by the new methods here presented to improve the performance of other experimental factors—as further described in the following paragraph.

C. Indirect-domain resolution enhancement: A homonuclear correlation example

As pointed out earlier [Eq. (5)], the mutual relations between the two spectral dimensions of the spatial encoding method often require compromises: for instance, decreasing the indirect-domain resolution and/or spectral width in favor of the direct-domain frequency BW. An example of such tradeoff is shown in Fig. 7 with a homonuclear spatially encoded 2D TOCSY experiment performed on a tyrosine ethyl ester sample. The relatively large SW_1, SW_2 values (>6 ppm) required to cover the full spectral range of this compound demand both a short gradient oscillating period T_a and a large acquisition k-range k^{max}. In order to achieve these spectral BWs and an acceptable direct-domain resolution, while keeping the experiment compatible with the available gradient's performance, a tradeoff has to be set with respect to the extent allowed for the indirect-domain evolution. As shown in Fig. 7 this calls for shortening the t_1^{max} encoding period to ~3 ms, even then, at the expense of demanding

the application of a relatively strong oscillating $G_a \approx 26$ G/cm for $t_2^{max} > 100$ ms. Under such low ν_1 resolution conditions, multiple diagonal peaks and cross peaks remain unresolved [Fig. 7(b)]. This example highlights the built-in limitations of a generic approach like spatial encoding: although there are only seven sites to be correlated in this molecule, the k^{max} of this experiment had to be taken as $30L^{-1}$ to cover the full spectral width. This is a result of the method's linear mapping of the ν_1-domain into k-axis echoes: when dealing with a nonuniform spacing of the chemical-shifted peaks, this leads to a nonuniform echo distribution and a suboptimal use of the gradients. Moreover, even under these demanding G_a conditions, sites that are close together along the indirect domain end up yielding echoes with poor or no resolution.

By providing nonlinear Ω_1-shift/k-echo mapping functions, the spatial/spectral encoding schemes hereby proposed can alleviate this limitation. Even peaks that are close together in Ω_1 can then be resolved into clearly separated echoes along the k-axis. Examples of this are shown in Fig. 8, which illustrates the use of SSE sequences on tyrosine ethyl ester. Although using identical acquisition conditions as in the conventional 2D ultrafast spectrum of Fig. 7, a much higher ν_1 resolution is achieved in these SSE TOCSY experiments by evenly distributing the peaks so that all echoes are spaced at $\Delta k = 3L^{-1}$ increments. Such an increased spacing was relatively easy to obtain by moderate gradients, thanks to the large gyromagnetic coefficient of ^{1}H. On the other hand, and unlike in the heteronuclear SSE-based experiments, where sites were characterized by long T_2 times and an overall insensitivity to the order of their ν_1 encodings, this homonuclear experiment clearly shows that the order with which sites are addressed can considerably influence their echoes' amplitudes. Sites which were excited first (small site index) are of smaller intensity than those excited last (high site index), as can be appreciated by comparing the results obtained for different orders of site excitation [Figs. 8(b) and 8(c)]. This can be attributed to the presence of homonuclear J-couplings, which by amplitude modulating the time-domain evolution over the course of the encoding act during this time as a sort of an effective T_2 decay.

By contrast, these weighting heterogeneities should be absent upon implementing the PSE scheme. The 2D spatial/spectral pulse required for testing this was designed based on oscillatory trapezoidal gradient waveforms; mixing as well as acquisition parameters were taken to be identical to those employed in the SSE experiments [Fig. 9(a)]. The resulting PSE TOCSY 2D spectrum [Fig. 9(b)] clearly avoids the differential site attenuation due to its uniform encoding time. Moreover, when compared with the SSE implementation, it can be seen that the overall duration of the parallel spatial encoding pulse can be made considerably shorter: ~25 ms versus >100 ms in the serial case. This in turn can be used to endow the PSE 2D rf pulse with higher shift selectivity in its the ν_1 addressing, as well as with a better average SNR for the final 2D spectrum.

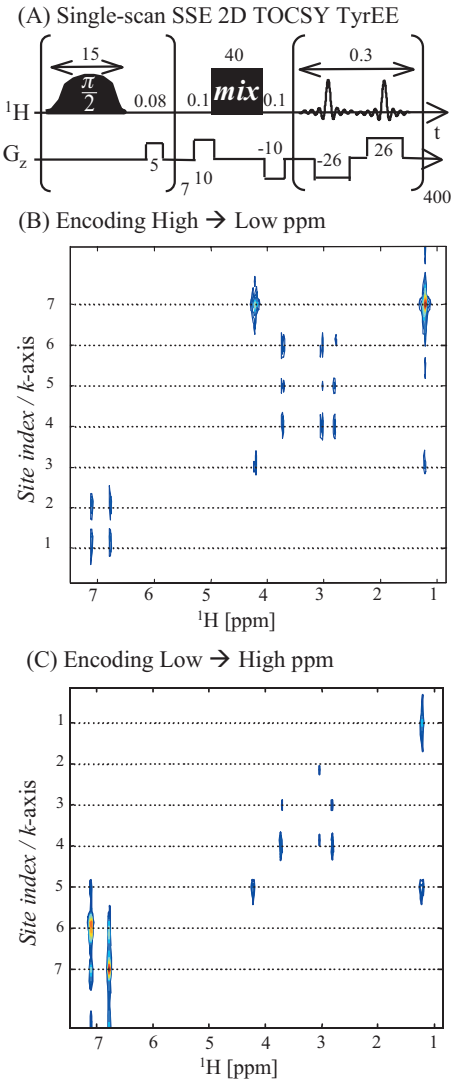

FIG. 8. (a) Homonuclear SSE-based 2D TOCSY pulse sequence based on an even distribution of the peaks along the k-axis. [(b) and (c)] 2D TOCSY NMR results on the same TyrEE sample as used in Fig. 7—including the same acquisition parameters but a SSE encoding. These two data sets differ by the order of excitation of the chemical sites. Notice (i) the enhanced indirect domain resolution that is obtained; (ii) the fact that due to the long encoding periods, sites that were excited first (lower k index) are also further attenuated due to T_2 relaxation and homonuclear J-modulation.

IV. DISCUSSION AND CONCLUSIONS

If available, *a priori* 1D information about the sample under investigation can help to construct more efficient forms of 2D NMR acquisitions. This has been amply documented for conventional 2D NMR experiments, where it is known that selective excitation can reduce the minimum number of acquisitions that are needed. In ultrafast schemes, where the 2D acquisition has already collapsed into a single scan, this kind of information can be traded for the sake of sensitivity or for improving spectral resolution. The present paper demonstrated two strategies that can bring about this flexibility, based on a serial and on a parallel spatial encoding of specific chemical sites. The serial scheme, characterized by maximal simplicity and minimal hardware demands, requires relatively long encoding durations and may thus be susceptible to differential weighting due to the sites address-

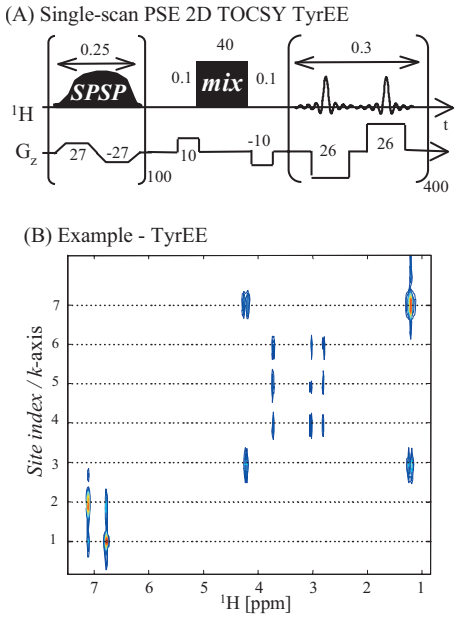

FIG. 9. Idem as in Fig. 8 except for the use of a PSE parallel addressing to encode the sites. The shorter overall encoding period prevented the undesired site-dependent attenuation; the shift selectivity is also better than in the SSE experiments given in Fig. 8.

ing order. If this is a limiting factor, an alternative parallel scheme can be employed; although characterized by increased hardware demands and by complex rf/gradient 2D waveforms, considerably shorter encoding periods as well as a uniform relaxation weighting are furnished by this scheme.

The key for executing this PSE approach is the design of new kinds of 2D spatial/spectral pulses for pure spectroscopic applications. Spatial/spectral pulses that exploit *a priori* known spectroscopic information have in fact been recently suggested for the realization of single-scan 2D Hadamard NMR experiments.[27] While in a conventional 2D Hadamard scheme the selected sites are endowed with a sign-alternating pattern that varies from scan to scan, the underlying principle behind its single-scan counterpart is to encode this set of experiments with a 2D spectral/spatial pulse. From this, distinct spatial regions and chemical sites will be endowed with signals of positive and negative signs. By requiring to excite neighboring spatial regions with opposite phases, however, the Hadamard approach puts forth harsher demands on the encoding gradients than the smoother, continuous winding patterns demanded by the PSE encoding. Moreover, the extraction of the spectral information requires the acquisition of sharp-edged images followed by a Hadamard-based postprocessing. The novel use of 2D spatial/spectral pulses hereby proposed for the PSE avoids this by choosing the simplest form that is suitable for the extraction of the spectral data: an echo train that in and of itself already represents the spectrum of interest.

An important advantage of the spectral/spatial schemes when compared with standard, continuous spatial encoding scheme is their insensitivity to diffusion. Indeed, achieving a high ν_1 resolution in the latter case requires relatively long $t_1^{\max}$ encoding periods in the presence of constant gradients; these conditions may lead to signal degradation due to diffusion effects.[28,29] On the other hand, when using either the very weak or the oscillating gradients demanded by the SSE or PSE, these effects become negligible. The spatial/spectral approaches are therefore suitable to deal with single-scan 2D experiments for highly diffusive compounds as well as in cases of microscopic turbulences. The reduced sensitivity to the latter can be a considerable aid to enhance the performance of ultrafast 2D NMR spectroscopy in combination with *ex situ* dynamic nuclear polarization (DNP), an experiment whereby hyperpolarized compounds are suddenly injected into the NMR spectrometer.[30,31] Furthermore, DNP-enhanced 2D NMR experiments are usually characterized by wideband, sparse ^{13}C/^{15}N indirect dimensions, and for them a single-scan acquisition is of essence. The potential of merging into DNP a SSE-like protocol has been very recently described.[32]

If multiple yet few scans are a possibility worth considering in a 2D acquisition, reductions in G_a going beyond those hereby described can be achieved. One could consider a multiple-scan hybrid scheme that combines a spatial/spectral Ω_1/k mapping strategy together with a folded encoding, where two or more spectral regions are put together to overlap within the same reduced k-range. Proper phase cycling may then be used to fully unravel a densely compacted mapping of broadband spectra. Further means to reduce the acquisition gradients could result by assuming sparseness along the direct domain; this may also enable the reconstruction of the full 2D spectrum by partial echo-planar spectroscopic-imaging procedure of minimal acquisition gradients. These and other applications are targets of ongoing studies.

ACKNOWLEDGMENTS

This research was supported by the Israel Science Foundation (ISF Grant No. 447/09), by a Helen and Kimmel Award for Innovative Investigation, and by the generosity of the Perlman Family Foundation. Y.S. acknowledges the Clore Foundation for a Ph.D. fellowship.

APPENDIX: DESIGN OF SPATIAL/SPECTRAL PULSES

2D spatial/spectral rf pulses are often used in *in vivo* applications to selectively excite a particular chemical species over an arbitrary geometry in space. The goal of such pulses in the present spectroscopic scenario is slightly different; hence we consider useful to introduce the basic principles of how these combined rf/gradient manipulations were here designed. Our goal was to simultaneously endow multiple targeted sites possessing different shifts with individually tailored spatial winding patterns. Analytically, this can be expressed as seeking a 2D transverse magnetization pattern of the form

$$M_{XY}(z,\nu_1)=\sum_{p=1}^{N}\exp[i(N-p+1)\cdot\delta kz]Q(\nu_1-\Omega_p). \quad \text{(A1)}$$

The method employed for this purpose is based on the linear approximation for pulse design,[25] according to which the

transverse magnetization created during the course of an excitation period T_{pulse} is

$$M_{xy}(z,\nu_1) \propto \int_0^{T_{\text{pulse}}} B_1(t) e^{i\nu_1(T_{\text{pulse}}-t)} e^{ik(t)z} dt, \tag{A2}$$

where $k(t)=\int_t^{T_{\text{pulse}}} \gamma_e G_e(t')dt'$ is defined by the gradient G_e used throughout the excitation. The availability of two degrees of freedom, t and $G_e(t)$, to "steer" the evolution of the spins during the course of the pulse enables one to use $B_1(t)$ for addressing arbitrary (z,ν_1) values. For a successful design of this spatial/spectral $B_1(t)$ pulse, one has first to determine the oscillatory gradient waveform $G_e(t)$ that will suit best the desired magnetization response. The main features to be taken into account in this design include (1) the gradient's oscillatory cycle, a period that will be inversely proportional to the maximum ν_1 spectral width that can be addressed without aliasing, (2) the gradient's amplitude, which together with the cycle's period will determine the spatial resolution of the pulse and, correspondingly, the maximal spatial winding that can be imposed, and (3) the overall duration of the pulse, which will define Q's spectral resolution.

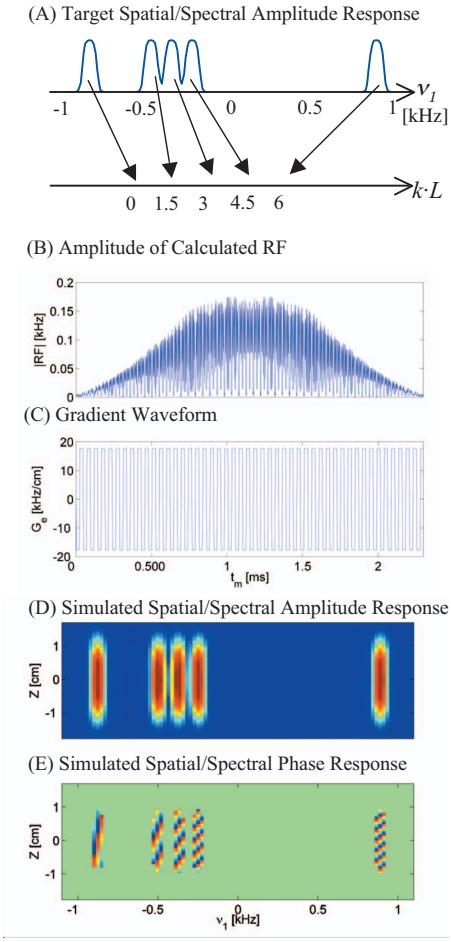

FIG. 10. Synthesis and typical performance of the 2D spatial/spectral rf pulse design algorithm. (a) Targeted spectral/spatial profile comprising three sites spaced relatively close together ($\Delta\nu_1=120$ Hz) and two additional more distant offsets. The desired spatial pattern was characterized by different k-wave-numbers for each site, spaced $\delta k=1.5L^{-1}$ increments apart. The 2D rf was designed using a 48-cycle oscillating gradient waveform with amplitude of ~17 kHz/cm (corresponding to 4 G/cm for ^{1}H) and duration of 23.04 ms [(b) and (c)]. Solving the Bloch equations for spins evolving under the designed rf and gradient waveforms provided a response very similar to the targeted one: (d) shows the amplitude response and (e) shows the phase response of the spins as a function of position for each chemical site.

When dealing with samples characterized by large spectral widths, the use of a minimal $\pm G_e$ gradient oscillation period makes the presence of excitation spectral aliasing unavoidable. A problem will then arise if these harmonic excitation bands coincide with a targeted spectral peak of interest. A natural solution to this issue, akin to that arising in DANTE sequences,[26] consists of exploiting "empty" spectral regions where no peaks are known to reside. By slightly modifying the design parameters one can "shift" these bands of harmonics; excitation aliasing can then be set to lie in empty regions, and any undesired spectral contributions are thus avoided.

Assuming these various parameters have been properly set, the targeted M_{XY} pattern in Eq. (A1) can be substituted into Eq. (A2), leading to a set of linear equations that relate the desired magnetization response with the required transmission B_1 rf as a function of time. In order to derive B_1, an inverse non-uniform Fourier transform operation is necessary. In this study we employed a method based on conjugate gradients[33] for the evaluation of this FT. The first stage in the resulting iterative search is to transform all the continuous variables involved—including the frequencies as well as the spatial positions and the excitation times—into discrete axes endowed with a sufficiently large number of N_Ω, N_z, and N_t points, respectively. Under this discretization, Eqs. (A1) and (A2) can be rewritten in a matrix form as

$$\underline{X} = T\underline{x}, \tag{A3}$$

where $(x)_m=B_1(t_m)$ with $m=1\cdots N_t$, $(X)_n=M_{XY}(\{z,\Omega_1\}_n)$ with $n=1\cdots(N_\Omega N_z)$, and $T_{nm}\propto e^{i\{\Omega_1\}_n t_m} e^{ik(t_m)\{z\}_n}$. The numerical solution for the rf shape $\{(x)_m\}_{m=1\cdots N_t}$ of Eq. (A3) was based on the following algorithm.

Given the Linear Relation: $X=T\cdot x$

Inputs: X—a vector of length P
T—a phasor matrix of size P×N
x_0—initial guess for the coefficient vector (of length N)
M–the number of iterations

Preliminary Calculations:
$\Delta_0=X-T\cdot x_0$
$p_0=q_0=T^H\Delta_0$, where T^H is the complex-conjugate of transverse (T).

for $l=0,\ldots$M do
$v_l=Tp_l$
$\mu_l=q_l^H q_l / v_l^H v_l$
$x_{l+1}=x_l+\mu_l p_l$
$\Delta_{l+1}=\Delta_l-\mu_l v_l$
$q_{l+1}=T^H\Delta_{l+1}$
$\xi_l=q_{l+1}^H q_{l+1}/q_l^H q_l$
$p_{l+1}=q_{l+1}+\xi_l p_l$

end for

Output: Vector of coefficients x_M

Usually, starting with an initial guess of zeroes as the x_0 vector, the algorithm converged rapidly and provided the de-

sired results within a very few (1–3) iterations. The resulting $B_1(t_m)$ shape was then ported to the spectrometer, and together with its accompanying $G_e(t_m)$ gradient waveform clocked out at its predefined $\Delta t = t_m - t_{m-1}$ dwell. An example of the desired and calculated spatial/spectral response for a five-site sample is shown for completion in Fig. 10.

[1] J. Cavanagh, W. J. Fairbrother, A. G. Palmer, N. J. Skelton, and M. Rance, *Protein NMR Spectroscopy: Principles and Practice* (Elsevier, New York, 2006).
[2] R. R. Ernst, G. Bodenhausen, and A. Wokaun, *Principles of Nuclear Magnetic Resonance in One and Two Dimensions* (Clarendon, Oxford, 1987).
[3] H. Kessler, M. Gehrke, and C. Griesinger, Angew. Chem., Int. Ed. Engl. **27**, 490 (1988).
[4] E. Kupce, T. Nishida, and R. Freeman, Prog. Nucl. Magn. Reson. Spectrosc. **42**, 95 (2003).
[5] J. Jeener, Lecture presented at Ampere International Summer School II, Basko Polje, Yugoslavia, 1971.
[6] W. P. Aue, E. Bartholdi, and R. R. Ernst, J. Chem. Phys. **64**, 2229 (1976).
[7] D. Jeannerat, Magn. Reson. Chem. **38**, 415 (2000).
[8] E. Lescop, P. Schanda, R. Rasia, and B. Brutscher, J. Am. Chem. Soc. **129**, 2756 (2007).
[9] P. Feng-Kui and R. Freeman, J. Magn. Reson. **48**, 519 (1982).
[10] E. Kupce and R. Freeman, J. Magn. Reson. **162**, 300 (2003).
[11] K. Kazimierczuk, W. Kozminski, and I. Zhukov, J. Magn. Reson. **179**, 323 (2006).
[12] N. Pannetier, K. Houben, L. Blanchard, and D. Marion, J. Magn. Reson. **186**, 142 (2007).
[13] S. Hiller, F. Fiorito, K. Wüthrich, and G. Wider, Proc. Natl. Acad. Sci. U.S.A. **102**, 10876 (2005).
[14] V. A. Mandelshtam, J. Magn. Reson. **144**, 343 (2000).
[15] J. C. Hoch and A. S. Stern, Methods Enzymol. **338**, 159 (2002).
[16] L. Frydman, T. Scherf, and A. Lupulescu, Proc. Natl. Acad. Sci. U.S.A. **99**, 15858 (2002).
[17] Y. Shrot and L. Frydman, J. Chem. Phys. **128**, 052209 (2008).
[18] P. Mansfield, Magn. Reson. Med. **1**, 370 (1984).
[19] M. Gal and L. Frydman, *Ultrafast Multidimensional NMR: Principles and Practice of Single-Scan Methods*, Encyclopedia of NMR Vol. 10, edited by D. M. Grant and R. K. Harris, doi:10.1002/9780470034590.emrstm1024 (to be published).
[20] L. Frydman, A. Lupulescu, and T. Scherf, J. Am. Chem. Soc. **125**, 9204 (2003).
[21] Y. Shrot and L. Frydman, J. Magn. Reson. **164**, 351 (2003).
[22] P. Pelupessy, L. Duma, and G. Bodenhausen, J. Magn. Reson. **194**, 169 (2008).
[23] P. A. Bottomley and C. J. Hardy, J. Appl. Phys. **62**, 4284 (1987).
[24] C. H. Meyer, J. Pauly, A. Macovski, and D. G. Nishimura, Magn. Reson. Med. **15**, 287 (1990).
[25] J. Pauly, D. Nishimura, and A. Macovski, J. Magn. Reson. **81**, 43 (1989).
[26] P. T. Callaghan, *Principles of Nuclear Magnetic Resonance Microscopy* (Oxford University Press, New York, 1994).
[27] A. Tal, B. Shapira, and L. Frydman, Angew. Chem. **121**, 2770 (2009).
[28] P. Giraudeau and S. Akoka, J. Magn. Reson. **192**, 151 (2008).
[29] Y. Shrot and L. Frydman, J. Chem. Phys. **128**, 164513 (2008).
[30] M. Mishkovsky and L. Frydman, ChemPhysChem **9**, 2340 (2008).
[31] L. Frydman and D. Blazina, Nat. Phys. **3**, 415 (2007).
[32] P. Giraudeau, Y. Shrot, and L. Frydman, J. Am. Chem. Soc. **131**, 13902 (2009).
[33] S. Kunis, Ph.D. thesis, University of Lubeck, 2006.
[34] Y. Shrot, A. Tal, and L. Frydman, Magn. Reson. Chem. **47**, 415 (2009).
[35] J. Pauly, P. Le Roux, D. Nishimura, and A. Macovski, IEEE Trans. Med. Imaging **10**, 53 (1991).